An Efficient Automatic Brain Tumor Segmenter

Idanis Diaz*, Pierre Boulanger*, Russell Greiner*, Bret Hoehn*, Lindsay Rowe† and Albert Murtha†

* Department of Computing Science, † Radiation Oncology Department
University of Alberta

***Abstract*— This paper introduces EABTS an efficient automatic method for segmenting multiple components of brain tumor using four magnetic resonance image modalities. EABTS's four stages involve automatic histogram multi-thresholding and morphological operations including geodesic dilation. Empirical results on 16 hand-segmented real tumors show that EABTS works very effectively, achieving a Dice accuracy of 81% in segmenting edema and 85% in segmenting Gross Tumor Volume (GTV).**

I. Introduction

Medical image segmentation provides information necessary for diagnosis, radiotherapy, treatment planning and assessment, disease monitoring, and surgery planning. This paper focuses on segmenting brain tumors in magnetic resonance image (MRI), distinguishing different components within the tumor volume.

In typically clinical practice, experts *manually* segment a volume, or use semi-automated tools. Unfortunately, such manual segmentation of tumors is time consuming and yields non-repeatable results [1]. Many semi-automatic tumor segmentation approaches have been reported in the literature [2, 3, 4]; however, few of these methods achieve the objectives most desired in clinical practices: *simplicity, accuracy, speed, and minimal user interaction*. Some semi-automatic segmentation methods are based on elementary image processing techniques, for example, thresholding, region growing, and edge detection. Some of these methods require numerous user interactions and their accuracy is affected by the lack of contrast at different tissues boundaries. Methods that involve robust statistic models or machine learning techniques, for instance, fuzzy clustering and k-nearest-neighbor, require precise input parameters and user result interpretations [2, 3, 4]. Other methods, based on deformable models, are very sensitive to the in-homogeneities present in the MR images and also require user guidance.

This paper presents an Efficient Automatic Brain Tumor Segmenter (EABTS) that does not require a user to provide input parameters nor initial estimations, nor requires any other user interaction, and is very simple to use. Our approach finds edema and Gross Tumor Volume (GTV) using the four standard clinical Magnetic Resonance Image (MRI) modalities: T1-weighted (T1), T1-weighted with gadolinium contrast agent (T1C), T2-weighted (T2), and Fluid Attenuated Inversion Recovery (FLAIR) [5]. The approach is based on an automatic histogram multi-thresholding procedure and morphological operations, including geodesic transformations [6]. Although segmentation methods based on histograms are very sensitive to the poor contrast at the tissue boundaries, EABTS overcomes this challenge by using the information provided by the different scans and with the use of double-thresholding at different grey levels and geodesic dilation.

Section 2 describes our segmentation method; each of its subsections explaining one component of the algorithm. Section 3 shows that EABTS works effectively on real MR images, producing results comparable to expert manual segmentations.

II. The EABTS Algorithm

Our EABTS segmentation algorithm takes as input four 3D registered volumes of the same patient containing the four standard MR sequences: T1, T1C, T2, and FLAIR. Then, EABTS applies the following four steps.

2.1 Thresholding

In this first stage, EABTS takes advantage of the known histogram shapes common to the vast majority of brain MRI scans. Generally, brain MRI histograms are bimodal: the first mode represents the most common intensity values found in the image background, which are close to zero; and the second mode is mostly composed of grey values found in brain tissues corresponding to gray and white matters (see Figure 1). We followed Brummer *et al.* [7] by localizing different thresholds in the four image histograms to obtain binary 3D masks designed to separate different regions of interest within the image – *e.g.*, background from foreground, or the skull from brain tissue or affected areas with high/low intensities from healthy tissues. In order to simplify the threshold localization, our approach uses a Savitzky-Golay FIR filter to obtain a smooth histogram envelope for each volume [8]. This filter preserves higher-order moments by approximating the data within a window with a high-order polynomial using a least-squares procedure [9].

After EABTS produces these smooth histogram envelopes, it then localizes the first and second modes, μ_1 and μ_2. Typically, the edema presents high intensity signal on FLAIR and T2, and the gadolinium-enhanced lesion presents high T1C intensities. Furthermore, most tumors have low signal intensity on T1.

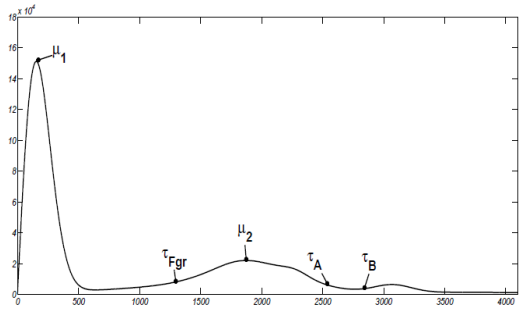

Figure 1: Bi-modal function with modes μ_1 and μ_2 and multiple thresholds: τ_{Fgr}, τ_A, and τ_B .

Table 1 summarizes some patterns that we have observed in brain tumor MRIs. These observations lead us to threshold the images after the second mode μ_2 to separate areas of high intensities from the rest of the brain tissues.

Table 1: Signal intensity for tumors in MRIs.

	Edema	**Gadolinium Enhanced Lesion**	**Skull**
T1	Low	Low	High
T1C	Low	High	High
T2	High	High	High
FLAIR	High	–	High

In particular, EABTS analyzes the first and second derivatives of the histogram envelopes after μ_2 and marks, as possible thresholds, the inflection points where the slope change directions. For each modality $m \in$ {T1, T1C, T2, FLAIR}, we define three main thresholds $\tau_{Fgr}(m)$, $\tau_A(m)$, and $\tau_B(m)$. Figure 1 illustrates the threshold locations. EABTS identifies τ_A as the point with the maximum slope changes sign, after the second mode μ_2. Each threshold highlights the skull's voxels on all the images (T1, T1C, T2, and FLAIR); they also identify the gadolinium-enhanced lesions on T1C, and ventricles, sulci, and edema on T2, as shown in Figure 2. For FLAIR, our approach localizes three thresholds, τ_A(FLAIR) as explained above, and τ_B(FLAIR), which is the first intensity value greater than τ_A (FLAIR), where a slope direction change also occurs. Figure 3 shows an example of the results obtained by thresholding FLAIR with τ_A(FLAIR) and τ_B (FLAIR). Both thresholds yield images containing part of the skull and edema. The image generated by τ_A(FLAIR) is taken as the geodesic mask and the image generated by τ_B (FLAIR) is taken as the marker set for the geodesic dilation operator [6].

The third threshold localized in FLAIR histogram is τ_{Fgr}(FLAIR), which corresponds to the first slope direction change found when descending the curve from μ_2 on the left side. This threshold selects voxels corresponding to brain tissues and skull, excluding ventricles, sinuses, and sulci. Figure 3 shows an image thresholded with τ_{Fgr}.

We represent the 3D image associated with a MRI modality m as $I(m) : \mathcal{R}^3 \rightarrow \mathcal{R}$ (*i.e.*, which gives an intensity value for each (x, y, z) point). Given a threshold $\tau \in \mathcal{R}$, we define a 3D mask:

$$M(m, \tau)[x] = \begin{cases} 1 & \text{if } I(m)[x] > \tau \\ 0 & \text{otherwise} \end{cases}. \quad (1)$$

We will rewrite $M(Tm, \tau_A(Tm))$ as just $M(Tm, \tau_A)$. For example $M(T1, \tau_A)$ contains all the voxels whose T1 intensities are greater than the value of τ_A(T1).

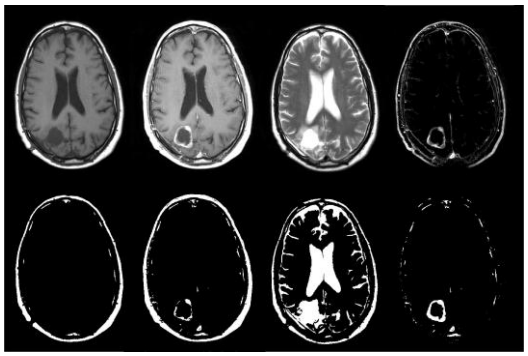

Figure 2: Thresholding results on one slice. On the top row from left to right: T1, T1C, T2, I_{T1C-T1}. On the bottom row from left to right, the thresholding results for A(T1), A(T1C), A(T2) and the enhanced lesion from I_{T1C-T1}.

Figure 3: Thresholding results on one slice from FLAIR. From left to right is the slice in FLAIR, the result of thresholding with τ_{Fgr}(FLAIR), the results obtained by thresholding with τ_A(FLAIR) and τ_B(FLAIR).

2.2 Skull Segmentation

EABTS extracts a first approximation of the skull location by selecting the biggest 3D-connected component from $M(T1, \tau_A)$, then complementing it with $M(T1C, \tau_A)$ to produce a mask M_{skull} containing only the skull. This mask is removed from all the images *i.e.*, all of the subsequent masks consider just the volume within the skull.

2.3 Edema Segmentation

The two masks M (FLAIR, τ_A) and M (FLAIR, τ_B) contain voxels corresponding to the tumor edema. EABTS applies a geodesic dilation operator where M (FLAIR, τ_B) is the marker and M' (FLAIR, τ_B) is the geodesic mask [6]. As illustrated in Figure 3, in M (FLAIR, τ_B) the edema is less defined in comparison to M (FLAIR, τ_A). However, M (FLAIR, τ_A) often contains small regions that do not belong to the tumor but are still often 3D-connected, while M (FLAIR, τ_B) provides less

information but it has fewer of these small regions. For this reason, EABTS takes the edema from M (FLAIR, τ_B) as a seed in the geodesic dilation process until the edema area in M (FLAIR, τ_A) is reached.

Sometimes M (FLAIR, τ_A) does not identify the edema completely because the presence of cyst and necrosis perturb the signal intensity in the FLAIR image. To overcome this challenge, EABTS also extends the seeds by geodesic dilation over M (T2, τ_A). The geodesic dilation is performed after eliminating ventricles and sulci using M(T2,τ_A) ∩ M (FLAIR,τ_{Fgr}). As the τ_{Fgr} threshold separates regions with low intensities (such as ventricles, sulci, sinuses, etc.) from tissues and skull, the image resulting from the intersection contains only voxels that correspond to the edema and some other isolated small areas with high intensity values in T2. Thus, the geodesic dilation operator is able to complement the initial edema estimate from FLAIR with information provided by T2.

2.4 GTV Segmentation

Although τ_A(T1C) helps to identify the GTV, we complement this initial segmentation with information extracted from I_{T1C-T1} = T1C − T1, which is the image formed by a voxel-wise subtraction of the intensities of T1 from T1C (see Figure 2). At this stage, EABTS does the following:

1. Standardize the intensity values of T1 and T1C to a common intensity scale by using the method proposed in Nyúl and Udupa [10].
2. Select from I_{T1C-T1} the voxels with high intensities that are 3D-connected with the GTV from M(T1C, τ_A) and the edema mask obtained in the previous stage.

EABTS standardizes the intensity values to cancel areas that correspond to the healthy tissue and to enhance voxels corresponding to the enhanced contrast.

III. Segmentation Results

3.1 Patients Data Sets

The MRI dataset used in this work are from patients with glioblastoma, at different stages, treated at the Cross Cancer Institute (CCI) in Alberta, Canada. We developed EABTS using sixty patient cases, each containing only axial slices, in each of the 4 sequences T1, T1C, T2, and FLAIR that were acquired with a 1.5T MR Philips Intera Achieva scanner using a resolution of 512×512 voxels with 21 to 25 slices (depending on each data set), and with a spatial resolution of 1 × 1 × 5 mm. All MRI data were previously stripped of all patient personal information.

3.2 Evaluation

A team of radiation oncologists from CCI hand-segmented edema and the GTV for sixteen random cases (different from the sixty used during the development stage). We then ran EABTS on these cases to produce edema and GTV masks, using the parameters learned from the 60 training instances and did not tune the parameters on these new instances. For each image, we then computed the similarity between the mask M produced by our method with respect to the corresponding image E segmented by the experts, using the Dice coefficient:

$$D(M, E) = (2 \times TP)/((2 \times TP) + FP + FN) \quad (3)$$

where TP, FP and FN are respectively the number of voxels that are true positive, false positive, and false negative.

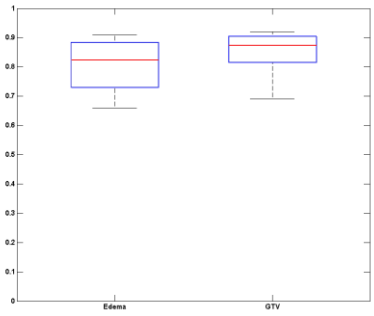

Figure 4: A box plot of the Dice coefficients obtained for the edema and GTV segmentations.

Figure 4 shows a box plot of the Dice coefficients obtained for the sixteen evaluation cases, for both the edema and GTV segmentations. The average Dice coefficient for Edema and GTV are 81% and 85% respectively. Figure 5 shows slice examples of the segmentations obtained for the best and the worst evaluated cases.

One can see that, in general, EABTS did extremely well, on essentially every volume. The few exceptions happened when the images from different modalities were not well registered or in the case when the image did not satisfy the rules given in Table 1. Both problems are easy to address: one can solve the first problem by running a registration step to align the modalities, which is easy as they are from

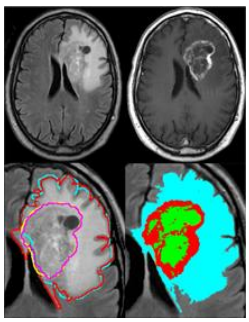

(a) A slice form the best segmentation

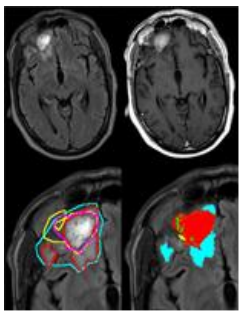

(b) A slice from the worst segmentation

Figure 5: The top images are the original slices in FLAIR and T1C. On the bottom left, edema: manual in cyan and automatic in red lines; GTV: manual in yellow and automatic in magenta lines. The bottom right image shows the segmentation obtained by EABTS: edema in cyan, GTV in green and enhanced contrast in red.

the same person at the same time. The worst case in Figure 5 is caused by the presence of high intensity levels covering the tumor area in some slices in the T1 sequence; this can be fixed by a better tuning of the MRI machine.

IV. Conclusion

Although the image set selected to evaluate EABTS includes some challenging cases, the average Dice Coefficients of 81% and 85% show extremely high overlap between the manual and automatic segmentations for edema and GTV accuracies that are comparable to the average dispersion between two trained radiation oncologists [11]. EABTS is also very fast, requiring only one minute to segment each case.

This paper presents a fast, automatic and accurate method for segmenting brain tumors. As it identifies thresholds based on the histograms of intensities present in the images, the EABTS method is easily able to effectively segment images produced from different protocols and scanners.

V. Acknowledgements

The authors wish to thank to Helene Daly, Colin Field, Juliette Jordan, and Heather Warkentin for their help with respect to the manual identification, extraction and processing of the data.

References

[1] G. Mazzara, R. Velthuizen, J. Pearlman, H. Greenberg, and H. Wagner, "Brain tumor target volume determi- nation for radiation treatment planning through auto- mated MRI segmentation," *Int. J. Radiat. Oncol.*, vol. 59, 2004.

[2] D. Pham, C. Xu, and J. Prince, "Current methods in medical image segmentation," *Annu. Rev. Biomed. Eng.*, vol. 2, 2000.

[3] P. Cattin, M. Harders, J. Hug, R. Sierra, and G. Szekely, "Computer-supported segmentation of ra- diological data," in *Biomedical Image Analysis - Seg- mentation Models*. 2005.

[4] I. Bankman, *Handbook of Medical Image: Processing and Analysis*, 2008.

[5] Jerrold Bushberg, Anthony Seibert, Edwin Leidholdt, and John Boone, *The Essential Physics of Medical Imaging*, 2nd edition edition, Dec. 2001.

[6] P. Soille, *Morphological Image Analysis: Principles and Applications*, Springer, 2010.

[7] M. Brummer, R. Merserau, R. Eisner, and R. Lewine, "Automatic detection of brain contours in MRI data sets," vol. 12, June 1993.

[8] A. Savitzky and M. Golay, "Smoothing and Differenti- ation of Data by Simplified Least Squares Procedures," *Anal. Chem.*, vol. 36, 1964.

[9] P. Persson and G. Strang, "Smoothing by Savitzky- Golay and Legrend Filters," in *Mathematical Systems Theory in Biology, Communications, Computation and Finance*. 2003.

[10] L Nyúl and J. Udupag, "On standardizing the MR image intensity scale," *Magn. Reson. Med.*, vol. 42, 1999.

[11] M. Schmidt, "Automatic brain tumor segmentation," M.Sc. thesis, University of Alberta, 2005.